BNL-62935
INFORMAL REPORT

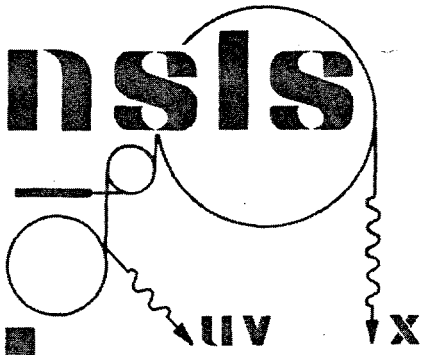

Data Acquisition and Analysis of Mammography Images at the NSLS June - August 1995

F. Arfelli, C. Burns, D. Chapman, N. Gmur, R. E. Johnston, R. Menk, E. Pisano, D. Sayers, W. Thomlinson, D. Washburn, Z. Zhong

NATIONAL SYNCHROTRON LIGHT SOURCE

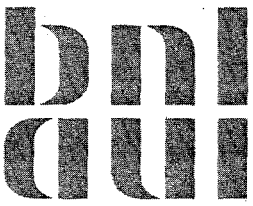

BROOKHAVEN NATIONAL LABORATORY
ASSOCIATED UNIVERSITIES, INC.
Under Contract No. DE-AC02-76CH00016 with the
UNITED STATES DEPARTMENT OF ENERGY

Data Acquisition and Analysis of Mammography Images at the NSLS June - August 1995

F.Arfelli[1], C.Burns[2], D.Chapman[1,4], N.Gmur[1], R.E.Johnston[2], R.Menk[1], E.Pisano[2], D.Sayers[3], W.Thomlinson[1], D.Washburn[2], Z.Zhong[1]

1. NSLS, Brookhaven National Laboratory, Upton, NY, 11973
2. Department of Radiology, University of North Carolina, Chapel Hill, N.C.27599
3. Department of Physics, North Carolina State University, Raleigh, N.C.27695
4. Illinois Institute of Technology, Chicago, I1 60616

1. Introduction

The display of low-contrast tissue structures and the finest microcalcifications is essential for the early diagnosis of breast cancer (1,2,3). From this requirement, it should be noted that the x-ray imaging beam energy must be matched to the object thickness and the tissue composition of the breast in order to achieve high image quality with minimum radiation exposure to the patient (4-10). With the conventional molybdenum anode x-ray tube, widely used for approximately the last 20 years, the possibilities of adapting the beam energy to the object thickness or the density of the breast tissue are severely limited since the relative energy distribution of the x-ray spectrum changes very little by varying the x-ray tube voltage.

The synchrotron radiation x-ray source provides a high flux over a wide continuous energy spectrum. This presents the possibility of obtaining a monochromatic tunable beam in order to choose the optimal energy that can increase the information content in the images or reduce the patient exposure. The intrinsic vertical collimation of the synchrotron beam may reduce the scattered radiation. Anti-scattering grids used in the conventional mammographic system are not necessary. They may absorb more than 50% of the x-rays exiting from the breast, causing the dose to be more than doubled in order to maintain image quality.

At Brookhaven National Laboratory mammography experiments are being carried out at the X27C R&D beamline of the National Synchrotron Light Source using a monochromatic x-ray beam in order to explore the potential of monoenergetic photons for mammographic imaging. Preliminary reports of some of the work have been submitted for publication as conference proceedings (11,12). Our measurements and results occurred during two separate one week periods of beam time; the first one in June and the second one in August 1995.

The monochromatic x-ray beam used for the imaging was produced by a double crystal Si(111) Bragg monochromator which can select energies from 15 to 25 keV. Conventional mammographic phantoms, including a contrast-detail phantom, the

ACR (American College of Radiology) phantom and an in-vitro excised tissue sample, were imaged. The detector was a Fuji Image plate with a spatial resolution of 100 microns. Many images of the same phantoms were also recorded on a conventional mammographic film-screen system. The images were acquired in a line scan mode simultaneously moving the phantom and the detector through the beam. These images were compared with images produced using a conventional mammographic system at the University of North Carolina. The synchrotron images show a better contrast than the conventional images when compared to the theoretical contrast.

2. Experimental set-up

The experimental set-up is shown in Figure 1. The overall length of the system from the monochromator to the detector is 2.8 meters. The 85 mm wide white beam is provided by the X27C bending magnet source roughly 20 meters from the experimental hutch. The set-up, that is not under vacuum, begins downstream of a beryllium window. At that point a slit provides a 0.5 mm high beam which is incident on a double crystal Si(111) Bragg monochromator. The monochromator consists of two independent crystals 150 mm wide providing complete horizontal acceptance of the beam. The lengths of the first and second crystals are 60 mm and 90 mm, respectively, chosen in order to allow a vertical acceptance up to 3 mm in the energy range from 15 to 25 keV (corresponding to a Bragg angle range from 7.6 to 4.5 degrees). The energy resolution $\Delta E/E$ is 5×10^{-4} at 18 keV. The monochromator aluminum chamber is kept in a He atmosphere. The first water-cooled crystal holder is attached to a Huber rotational stage which allows the Bragg angle to be set with an angular resolution of $2.5*10^{-4}$ deg. The beam diffracted by the first crystal has another Bragg reflection from the second crystal set in parallel configuration in order to keep the outgoing beam parallel to the incident beam but with an offset in the height which is about 20 mm (about twice the distance of 10 mm between the crystals). There is a slightly variation in the height when changing the Bragg angle but it is negligable for our purposes. The second crystal holder is fixed to the same frame as the first one in order to rotate the two crystals simultaneously. It is provided with fine adjustments by means of three remote-controlled micrometric screws moved by a piezo with a resolution of 0.1 micron (Picomotor driver, New Focus). With these adjustments a good alignment of the two crystals can be achieved. That is fundamental for maximizing the transmitted flux and obtaining a uniform beam over its width. The energy calibration of the monochromator is done by measuring the k-absorption edges of Mo and Rh foils. Each time the working energy is changed the correct position of the second crystal is checked with a fine scan until the maximum flux transmission is reached. That means that a good overlap of the rocking curves of the two crystals exists.

At the exit of the monochromator the beam is collimated by lead shielding. Downstream of the monochromator there is a fast shutter with an ionization chamber in front of it which is used to monitor the strength of the incoming beam before opening the imaging shutter. Another slit is located downstream of the shutter,

approximately 110 cm in front of the object to be imaged. The dose monitor ionization chamber is placed after this slit and is used to measure the entrance dose to the phantom (Section 4). The detector is placed about 100 cm downstream of the phantom with a final slit just in front of it to reduce the scattered radiation from the phantom on the image plate. The detector and phantom are fixed on the same support and are moved vertically by a Klinger stepper motor driver.

3. Method

The detector is a Fuji ST3 PSP image plate used with a Fuji BAS 2000 image plate reader. Typical reading parameters are: sensitivity of 4000 or 400, latitude of 4 and a resolution size of 100 microns. The plates are read out as a 2048x2560 matrix (100 microns/pixel). Conventional mammographic film has also been used to record the images in conjunction with a Film Quick-CT film processor. Since the beam size is 0.5 mm high x 85 mm wide the images were acquired in line scan mode. The phantom and the detector, placed on the same vertical movement stage, were moved simultaneously through the beam by the stepper motor driver with a maximum speed of 16 mm/sec.

Data acquisition software has been developed to automate all the control and scan procedures. The input parameters required are: the beam energy, beam width, the phantom and filter thicknesses, the starting and final positions for the scan and the scan speed. The speed can be set directly or can be automatically chosen by the program for a predetermined detector exposure or, optionally, for a predetermined entrance dose to the phantom. The procedure reads the output current from the monitor ionization chamber (the one upstream of the fast shutter) and calculates the necessary speed. The current from the ionization chamber is amplified by a Keithley amplifier with the gain set at 10^9 and the output voltage is converted into counts/sec by means of a voltage-to-frequency converter which is connected to a scaler. Knowing the current I from the counts/sec, the relationship between the incident photon number/sec N_I and the current I from the ionization chamber is the following:

$$N_I = \frac{I\omega_{ion}}{Ee(1-e^{-\mu_{en}^{gas}d})}$$

where E is the beam energy, e is the electron charge, ω_{ion} is the ionization energy for the gas in the chamber (nitrogen at atmospheric pressure), μ_{en}^{gas} is the absorption coefficient of the gas and d is the thickness of the ionization chamber.

The total photon number N_{tot} per cm^2 for a translation length h, a beam width w and a translation time ΔT is

$$N_{tot} = \frac{N_I \Delta T}{w\, h} = \frac{N_I}{s\, w}$$

where s is the scan speed. The requirements on detector exposure or phantom entrance dose are correlated to the incident photon number N_{tot} by means of the relationships shown in Section 4. In this way the scan speed is determined from a given N_{tot}. Thus, it is possible to increase or decrease the exposure by controlling the speed. There is, however, an intrinsic limit which is the maximum speed available and this means that the use of lucite and aluminum filters may be necessary directly after the monochromator.

When the scan starts, there is an acceleration phase arranged in such a way that the driver reaches the constant predetermined speed at the starting position at which time the shutter is opened. When the scan is at the end position the shutter is closed and the deceleration phase occurs. In practice, the total translation length is larger than the actual imaged phantom height to allow an imaging scan phase with constant speed and uniform exposure. For each run all the parameters used in the scan and the counts from the first and second ionization chambers are stored in a data file for off-line calculation.

The second ionization chamber (dose monitor chamber), placed after the fast shutter, measures the actual incident photon number on the phantom surface and from this measurement all the actual dose and exposure evaluations are performed, as described in Section 4. A scaler integrates the monitor chamber counts over the whole scan time corresponding to a total charge Q_{tot} produced in the ionization chamber by the incident beam. The actual incident photons/cm^2 N_{inc} is then given by:

$$N_{inc} = \frac{1}{hw} \frac{Q_{tot} \omega_{ion}}{Ee(1 - e^{-\mu_{en} d})}$$

where the product h*w represents the imaged area.

4. Dosimetry

Although mammography is uniquely effective in early detection of breast cancer, breast tissue is sensitive to radiation carcinogenesis. Although the resulting benefits of this examination substantially exceed potential risks, the dose must be monitored and minimized. Five major variables affect the breast dose delivered in a mammographic examination: the choice of the imaging system, the x-ray beam energy (HLV), the degree of breast compression employed and the breast size and adiposity.

Various dose parameters that might be considered are the in-air exposure at the position of the entrance surface of the breast (X_a), the dose to the entrance surface of the breast (D_s), the dose to the midline of the breast (D_{mid}), and the mean dose to the glandular tissue of the breast (D_g). In-air surface exposure is easy to measure with an ionization chamber and from this measurement it is easy to determine the surface dose but it gives an overestimation of the cancer risk. Midline dose is difficult to measure

directly (it can represent the risk to the glandular tissue) but it is an underestimation of the risk for the low-energy beams used for film-screen mammography. Mean glandular dose provides the best indicator of the potential carcinogenic radiation risk to the patient from mammographic examination. It commonly is assumed that the cancer risk is linearly related to the dose and that the breast cancers arise in the glandular tissue which is the most vulnerable when compared to adipose, skin and areolar tissues. Mean glandular dose cannot be measured directly but must be calculated from the result of simple measurements and tabulated values. The exposure as a function of the depth may be measured in phantoms using thermoluminescent dosimeters (TLD). Then the doses can be calculated from exposure levels using exposure-to-dose conversion factors.

Although the average glandular dose is the quantity usually reported, dose is sometimes given as the normalized average glandular dose (D_{gN}), which is the dose (D_g) normalized to the unit exposure in air at the entrance surface of the breast (X_a). The value X_a is set depending upon the detection system sensitivity in order to achieve a desired final image density. Once the exposure in air X_a is measured, then it is multiplied by the values of D_{gN} to arrive at reasonably accurate estimates of the average glandular dose (D_g) to the patient. For conventional mammography the normalized dose D_{gN} is determined by the HVL and breast thickness. Tables of values have been provided by a number of sources, including the National Council on Radiation Protection and Measurements (13) and the Center for Devices and Radiological Health (14).

A simplified model for the human breast used for dosimetry is proposed by Hammerstein et al. (15) to compute the average glandular dose in a firmly compressed breast with a rectangular cross section. The assumptions are that there is an outer layer of adipose tissue, not containing glandular tissue, that is roughly 0.5 cm thick on the outer (upper and lower) surfaces of the breast and there is a central portion of breast tissue composed of a uniform mixture of 50% adipose and 50% glandular tissue. Typical breast thickness after firm compression is 45 mm, although thickness can vary in a range from 15 mm to 75 mm.

In our mammographic experiments with synchrotron radiation it has been possible to implement a procedure for dose and exposure evaluations for each acquired image. We use simple relationships which consider the monoenergetic spectrum as well as the good geometric conditions due to the laminar beam and the slit system.

As shown above (Section 3), it is possible to determine the number N_0 of incident photons per surface unit (impinging on the phantom) from the output signal of the second ionization chamber, at a given energy E. The procedure developed for the estimation of dose determines N_0 (ph/cm^2), then the entrance dose to the lucite phantom is calculated, using the relationship:

$$D_s = N_0 \, E \, \frac{\mu_{en}^{luc}}{\rho^{luc}}$$

where μ_{en}^{luc} is the absorption coefficient of the phantom and ρ^{luc} is its density. In order to have a standard comparison of doses (since the thickness t of lucite can be different

at the different energies to allow a fixed exposure to the detector) the procedure calculates the entrance dose for a 42 mm thick lucite phantom, using $N_0' = N_0 e^{-\mu_{luc}(t-4.2)}$ instead of N_0 as incident flux, where μ_{luc} is the lucite attenuation coefficient.

The procedure also provides the exposure to the detector, E_D, using the relationship:

$$D_{air}(rad) = 0.877\, E_D(R) = N_D\, E \frac{\mu_{en}^{air}}{\rho^{air}}$$

where $N_D = N_0 e^{-\mu_{luc} t}$ is the photon number per surface unit reaching the detector.

Finally, the procedure calculates the average glandular dose that should be delivered to a breast of thickness t in order to obtain an image corresponding to a given exposure to the detector. The breast thickness usually taken into consideration is t = 45 mm, which is standard, as well as t = 20, 40, 42, and 70 mm.

Considering the standard breast composition described above and the breast thickness t, the photon number on the detector, N_D, for an image is related to the incident photon flux per unit surface area of the breast, N_t, by the relationship

$$N_D = N_t e^{-\mu_{adip}} e^{-\mu_{mix}(t-1)}$$

where μ_{adip} is the adipose tissue attenuation coefficient and μ_{mix} is the glandular-adipose mixture attenuation coefficient. The assumption is that the beam is attenuated by 1 cm of adipose tissue (considering both of the outer adipose layers in the breast) and by (t-1) cm of mixture tissue.

Then the glandular dose $D_g(x)$ at the depth x is calculated to a small mass of glandular tissue embedded in a homogeneous medium with standard composition (50% adipose and 50% glandular tissue):

$$D_g(x) = N_t E \frac{\mu_{en}^{gland}}{\rho^{gland}} e^{-\mu_{adip} 0.5} e^{-\mu_{mix}(x-0.5)}$$

where μ_{en}^{gland} and ρ^{gland} are the glandular tissue absorption coefficient and density, respectively.

The beam intensity at the depth x is attenuated by 0.5 cm adipose tissue and (x-0.5) cm mixture tissue. The mean glandular dose $\overline{D}_g$ is now evaluated integrating the glandular dose $D_g(x)$ over the breast mixed tissue region and dividing this number by the thickness:

$$\overline{D}_g = \frac{1}{(t-1)} \int_{0.5}^{t-0.5} D_g(x) dx$$

5. Theoretical considerations

In general the concept of 'image quality" can be considered to indicate the accuracy with which details can be perceived in an image. To avoid confusion about what this means it is necessary to define some terms and relationships which can lead to quantitative evaluation of the visibility of details in an image (16, 17).

A uniform photon fluence N_i (photons per unit area) is incident on a phantom which has two adjacent regions. Region 1 consists of a thickness t of a uniform material in the phantom without details whose total attenuation coefficient is $\mu(E)$. Region 2 is the region which contains the detail and it consists of a thickness (t-t') of the same material plus a thickness t' of a material whose attenuation coefficient is $\mu'(E)$. The transmitted photon fluences for the regions 1 and 2 are labeled N_{T1} and N_{T2}, respectively.

The contrast C in an image can be defined as the difference in x-ray transmission through region 1 and region 2 divided by the average of the two transmitted photon numbers:

$$C = \frac{N_{T1} - N_{T2}}{(N_{T1} + N_{T2})/2}$$

For a polychromatic beam we have to integrate over the energy and the contrast is:

$$C = \frac{\int_E N_{T1}(E)dE - \int_E N_{T2}(E)dE}{(\int_E N_{T1}(E)dE + \int_E N_{T2}(E)dE)/2}$$

The transmitted x-ray fluences, N_{T1} and N_{T2}, consist of a primary (unscattered) component, N_{P1} and N_{P2}, and a scattered component, N_{S1} and N_{S2}, respectively such that

$$N_{T1} = N_{P1} + N_{S1} \quad \text{and} \quad N_{T2} = N_{P2} + N_{S2}$$

In the case of a monochromatic beam at a given energy the primary radiation is

$$N_{P1} = N_i e^{-\mu t}$$

and

$$N_{P2} = N_i e^{-\mu(t-t')} e^{-\mu' t'}$$

Considering an equal contribution of scattered radiation that means $N_{S1} = N_{S2} = N_S$, the contrast becomes

$$C = \frac{2(1 - e^{-\Delta})}{1 + e^{-\Delta} + (2F/(1-F))}$$

where $\Delta = t'(\mu'-\mu)$ and the factor F is the scatter fraction defined as $F = N_S / N_{T1}$.

If the contribution of scattered radiation is uniform over the image, the number of scattered photons cancels in the numerator but it is present in the denominator, resulting in lower contrast. In the absence of scattered radiation the contrast depends only on the energy and on the absorption differences between the two materials (detail thickness, atomic number and density).

In the absence of scattered radiation and in the case of low contrast, C may be written

$$C \cong (\mu'-\mu)t'$$

In mammography the contrast is an important parameter because of the subtle differences in the transmission properties of the normal soft tissue and pathologic soft tissue masses and because of the importance of detecting minute details such as microcalcifications.

It is important to point out that radiographic contrast is actually influenced by two factors: the subject contrast and the receptor contrast. In the above considerations the concept of contrast refers to the subject contrast in which only the distribution of the photon intensity transmitted through the object is taken into consideration. We can suppose that the photons are counted by an ideal detector with efficiency 100%. The receptor contrast takes into consideration the x-ray intensity pattern related to the image pattern detected by the detector. In this case, instead of the photon numbers N_{T1} and N_{T2}, the corresponding output signal from the detector must be considered. For a film-screen system the x-ray intensity pattern is related to the optical density pattern in the mammogram. The receptor contrast is affected by the film type and the processing conditions. For a digital detector with a simple linear relationship between the incident fluence N_0 and the output signal $N_D = pf\varepsilon N_0$, the subject contrast and the receptor contrast are the same. (p is the pixel area, f is the conversion factor of the signal and ε is the detector efficiency). This relation holds only for monochromatic photon beams without scattered radiation since, in general, f and ε are energy dependent.

Image formation is a statistical process which involves the detection of a large number of photons. The inherent limitation to image information content is the statistical noise. The noise is generated in each component of an image system. It is possible to display all the image information content down to the appearance of "quantum mottle" which is the manifestation of the statistical noise.

A parameter which takes into consideration the effect of the noise on the image quality is the signal-to-noise ratio (SNR). Considering the SNR_{in} at the input to the detector (or considering an ideal detector with efficiency 100%) for a detail with area A, and the photon numbers transmitted in regions 1 and 2 ($n_{T1} = AN_{T1}$ and $n_{T2} = AN_{T2}$), one finds

$$SNR_{in} = \frac{n_{T1} - n_{T2}}{\sqrt{n_{T1} + n_{T2}}} = \frac{C}{2}\sqrt{n_{T1} + n_{T2}}$$

The numbers of photons n_{T1} and n_{T2} vary according to a Poisson distribution with the noise equal to $\sqrt{n_{T1}}$ and $\sqrt{n_{T2}}$ respectively, which is the standard deviation of the photon number.

This equation shows that, unlike the contrast, the signal-to-noise ratio is dependent on the exposure as well as on the size of the detail because it is proportional to $\sqrt{AN_i}$. Scattered radiation, if it is able to enter the detector, produces a reduction of the SNR_{in}.

The SNR_{out} of an image produced by a detector with a given Detective Quantum Efficiency (DQE) is related to the SNR_{in} as following

$$SNR_{out} = \sqrt{DQE}\, SNR_{in}$$

6. Analysis

The acquired digital images have been processed by means of procedures created using the software "Interactive Data Language" (IDL) (18).

The images to be analyzed were acquired by means of an image plate detector (Section 3). This system is based on a photostimulable phosphor which can temporarily store an x-ray image. The stored x-ray pattern is subsequently read out by a scanning laser beam, which converts the trapped energy into photostimulated luminescence. The emitted luminescence, which is proportional to the absorbed x-ray intensity, is detected by a photomultiplier whose output signal is logarithmically amplified and digitized with a 12-bit A/D converter. The gain of the logarithmic amplifier, which determines the range of the latitude, and the photomultiplier sensitivity (high voltage) are scaled according to the exposure level and the image contrast.

In the first phase of the analysis, the raw data, which are logarithmic values representing the A/D converter, are linearized using the following formula:

$$data_{lin} = \left(\frac{pixelsize}{100}\right)^2 * \frac{4000}{S} * 10^{L\left(\frac{Raw}{G} - \frac{1}{2}\right)}$$

where
L= Latitude (Dynamic Range; 1, 2, 3 or 4)
Raw = raw data value (0-255, 0-1023, or 0-4095)
G = total gradation level (256, 1024, or 4096)
S = sensitivity (400,1000, 4000, or 10000)
Pixel size = 100 or 200 microns

The parameters used in the June 1995 run were: L=4, G=1024, S=4000 and pixel size=100; in the August 1995 run they were: L=4, G=1024, S=400 and pixel size=100.

The image size was 85 mm (beam width) x 115 mm (translation length) in the June run, while it was 85 mm (beam width) x 95 mm (translation length) in the August run. Considering the pixel size of 100 microns, the number of image plate pixels per image was 850x1150 in the June experiment and 850x950 in the August experiment.

The phantoms used during the two experimental runs were the following: the ACR phantom (American College of Radiology), the CD phantom (Contrast-Detail), an anthropomorphic phantom (which simulates the breast tissue structures) and an excised breast tissue (the tumor was removed). Details of the ACR and CD phantoms are given in Figure 2.

The ACR phantom (Gammex: Model RMI 156) (Fig.2) is designed to attenuate x-ray beams in the same way as a human breast of 50% adipose and 50% glandular tissue compressed down to a thickness of 40 to 45 mm. Test objects of different sizes, shapes and densities are embedded in an insert. These test objects represent simulated malignancies such as micro-calcifications, fibrils and masses.

The CD phantom (Fig.2) is designed to evaluate the visibility limits of low contrast details of different thicknesses and diameter. It consists of a 15 mm thick Lucite background with circular areas of additional thickness. The circles are from 0.062 mm to 1 mm thick and the circle diameters are from about 0.3 to 7 mm. Thus, the two materials which determine the contrast are Lucite and air.

In the June experiment we imaged the CD, ACR and anthropomorphic phantoms using the following energies: 17, 18, 19.3, 20, 22, 24 keV. In the August experiment we imaged the CD and ACR phantom and the excised tissue at 16, 17, 18, 19 keV. In addition, imaging was done for the excised tissue at 20 and 22 keV and for the CD phantom at 24 keV.

The list in Table 1 summarizes the phantom images produced by the image plate in the June and August beamtime at the X27C beamline. It specifies the run number, the energy, the kind of phantom and the corresponding mean glandular dose normalized to a 45 mm thick breast.

The images of the CD and ACR phantoms have been processed in order to achieve a flat background cancelling artifacts due to horizontal and vertical non-uniformities in the incident beam intensity. The horizontal modulations are due essentially to a non-uniform transmission by the monochromator and the Be window, while the vertical modulations are due to periodic oscillations of the translation stage. In the August run the latter problem was nearly completely removed by changing the position of the image plate and phantom to a more stable configuration.

The CD phantom images have been used for contrast and SNR measurements for different detail thicknesses at different energies. The largest diameter details (7 mm) have been analysed. The concept of receptor contrast has been applied and this contrast has been compared with the theoretical subject contrast for a monochromatic beam without scattered radiation using the relationship in Section 5.

In order to calculate the contrast an IDL procedure has been implemented. Once an image is displayed on a screen the procedure draws a circle on same image. It is

possible to drag the circle on the image and change its diameter using the mouse. The first circle allows the selection of the detail area; then, the average value as well as the standard deviation of the pixels included into the circle is calculated. A rectangular box then appears and with the same operation it is possible to select and calculate the average value in a background area close to the detail. The procedure stores the results on a file and calculates the contrast. The SNR_{out} is determined using the photon fluence on the detectors.

The contrast for the same phantom details has been measured in three images of the CD phantom produced by a conventional mammographic x-ray tube at the University of North Carolina using a conventional film-screen as a detector and then digitized. The images were taken for phantoms of 15, 45, 75 mm thickness using 24, 25 and 30 kVp, respectively. The mean glandular dose is normalized to an exposure of 8 mR to the film.

Figure 3 shows the plot of the measured image plate contrast as a function of the detail thickness at 18 keV, along with the theoretical curve. In the same plot the contrast measurements for the digitized film are shown (45 mm thick phantom and 25 kVp). The measured monochromatic beam contrasts are in good agreement with the theoretical values, while the digitized film values are lower than theoretical values. The comparison between experimental and theoretical data for 17, 19.3, 20, 22, 24 keV is shown in Figure 4.

The plots of the measured contrast as a function of energy for three different detail thicknesses are compared with the theoretical curve in Figure 5. Good agreement is also obtained between the theory and experiment for the monochromatic data.

Conclusions

In two different periods of beamtime at the beamline X27C af the National Synchrotron Light Source at Brookhaven National Laboratory, we have performed preliminary studies of mammographic imaging using a monochromatic synchrotron radiation source. We used both phantom objects and real tissue samples.

Qualitative studies with the contrast-detail phantom show good agreement when compared with the theoretical contrast. As expected, the contrast is higher if the energy is lower. The results show an improved contrast with energies 18 keV and lower compared to images obtained from conventional polyenergetic x-ray imaging systems.

The results also show that for similar imaging conditions the monoenergetic mean glandular dose is less than that from polyenergetic sources. This is due both to the increased sensitivity of the image plate detectors and to actual reductions of dose for truely monochromatic beams.

Bibliography

1. L.H. Baker, "Breast cancer detection demonstration project: five-year summary report," CA 32(4) (1982) 194-225.

2. S.L. Saltzstein, "Potential limits of physical examination and breast self-examination in detecting small cancers of the breast: an unselected population-based study of 1302 cases," Cancer 54 (1984) 1443.

3. S. W. Fletcher, M.S. O'Malley and L.A. Bunce, "Physicians' abilities to detect lumps in silicone breast models," JAMA 251 (1984) 1580.

4. P.C. Stomper and R.S. Gelman, "Mammography in symptomatic and asymptomatic patients," Hem/Onc clinics NA, 3(4) (1989) 611-640.

5. X. Wu, E.L. Gingold, D.M. Tucker and G.T. Barnes, "X-ray spectral effects on contrast and dose in mammography," Med. Phys. 21 (1994) 1006.

6. F. Carrol, J. Waters, W. Andrews, R. Price, D. Pickens, R. Wilhott, P. Tompkins, C. Roos, D. Page, G. Reed, A. Veda, R. Bain, P. Wang and M. Bassinger, "Attenuation of monochromatic x-rays by normal and abnormal breast tissues," Investigative Radiology 29 (1994) 266-272.

7. E. Burattini, M. Gambaccini, P.L. Indovina, M. Pocek and G. Simonetti, "Synchrotron radiation: A new source in x-ray mammography," Radiol. Med. 4 (1992) 181-188.

8. E. Burattini, E. Cossu, C. DiMaggio, M. Gambaccini, P. Indovina, M. Maryianai, M. Porek, S. Simeoni and G. Simonetti, "X-ray mammography with synchrotron radiation: A new high resolution technique valid for clinical application," Radiology 195 (1994) 239-244.

9. A. Mantykentta-Pramanick and R. Carr, "High Resolution mammography with Synchrotron Radiation," Medical Physics, submitted for publication (1995).

10. J.M. Boone and J.A. Seibert, "A comparison of mono- and poly-energetic x-ray beam performance for radiographic and fluoroscopic imaging," Med. Phys. 21 (1994) 1853-1863.

11. R.E. Johnston, D. Washburn, P. Pisano, W.C. Thomlinson, L.D. Chapman, N.F. Gmur, Z. Zhong and D. Sayers, "Preliminary experience with monoenergietic photon mammography," Medical Imaging 1995: Physics of Medical Imaging, SPIE 2432 (1995) 434-441.

12. R.E. Johnston, D. Washburn, P. Pisano, C. Burns, W.C. Thomlinson, L.D. Chapman, F. Arfelli, N.F. Gmur, Z. Zhong and D. Sayers, "Mammography phantom studies with synchrotron radiation," Radiology, submitted for publication.

13. "Mammography: a user's guide." NCRP report 85. National Council on Radiation Protection and Measurements (Bethesda, Md, 1986).

14. B.J. Conway, ed. "Nationwide evaluation of x-ray trends (NEXT), tabulation, and graphical summary of surveys, 1984 through 1987." Conference of Radiation Control Program Directors, CRCPD publication 89-3 (Frankfurt, KY, 1989).

15. G.R. Hammerstein, D.W. Miller, D.R. White, M.E. Masterson, H.Q. Woodard and J.S. Laughlin, "Absorbed radiation dose in mammography," Radiology 130 (1979) 485-491.

16. R.J. Jennings, R.J. Eastgate, M.P. Siedband and D.L. Ergun, "Optimal x-ray spectra for screen-film mammography," Med. Phys. 8 (1981) 629-639.

17. J.W. Motz and M. Danos, "Image information content and patient exposure," Med. Phys. 5 (1976) 8-22.

18. Research Systems, Inc., Boulder, Colorado

Table 1a Run List (June 1995)

Run no.	Filename	Energy (keV)	Phantom	Average Glandular Dose(mrad)
1079	cd1.img	19.3	CD	67.9
1096	cd2_1096.img	18	CD	89.2
1118	cd3_1118_17kev.img	17	CD	146.9
1128	cd4_1128_20real.img	20	CD	48.5
1143	cd5_1143_22kev.img	22	CD	27.8
1155	cd6_1155_24kev.img	24	CD	20.4
1201	cd7_1201_18kev.img	18	CD	7.0
1203	cd7_1203_18kev.img	18	CD	21.3
1205	cd7_1205_18kev.img	18	CD	28.4
1207	cd7_1207_18kev.img	18	CD	45.5
1209	cd7_1209_18kev.img	18	CD	51.2
1211	cd7_1211_18kev.img	18	CD	64.1
1213	cd7_1213_18kev.img	18	CD	71.0
1215	cd7_1215_18kev.img	18	CD	99.7
1217	cd7_1217_18kev.img	18	CD	121.2
1090	acr1.img	19.3	ACR	40.1
1109	acr2_1109_18kev.img	18	ACR	67.2
1121	acr3_1121_17kev.img	17	ACR	137.5
1130	acr4_1130_20real.img	20	ACR	46.6
1149	acr5_1149_22kev.img	22	ACR	26.2
1159	acr6_1159_24kev.img	24	ACR	17.0
1080	ant1.img	19.3	ANTR	66.2
1113	ant2_1113_18kev.img	18	ANTR	73.5
1124	ant3_1124_17kev.img	17	ANTR	131.6
1133	ant4_1133_20real.img	20	ANTR	48.5
1151	ant5_1151_22kev.img	22	ANTR	25.8
1162	ant6_1162_24kev.img	24	ANTR	14.2

Table 1b Run List (August 1995)

Run no.	Filename	Energy (keV)	Phantom	Average Glandular Dose(mrad)
7019	cd_7019.img	16	CD	110.3
7026	cd_7026.img	17	CD	68.6
7029	cd_7029.img	18	CD	48.5
7032	cd_7032.img	19	CD	37.1
7034	cd_7034.img	24	CD	18.6
7014	acr_7014.img	16	ACR	105.4
7011	acr_7011.img	17	ACR	65.6
7008	acr_7008.img	18	ACR	45.9
7003	acr_7003.img	19	ACR	34.9
6010	bio_6010.img	18	TISSUE	96.8
6011	bio_6011.img	18	TISSUE	57.9
6012	bio_6011.img	18	TISSUE	155.3
6023	bio_6023.img	16	TISSUE	328.2
6026	bio_6026.img	17	TISSUE	164.6
6031	bio_6031.img	19	TISSUE	64.4
6036	bio_6036.img	20	TISSUE	37.3
6041	bio_6041.img	22	TISSUE	23.1
6106	bio_6106.img	16	TISSUE	106.9
6109	bio_6109.img	17	TISSUE	66.6
6112	bio_6112.img	18	TISSUE	47.1
6115	bio_6115.img	19	TISSUE	35.1

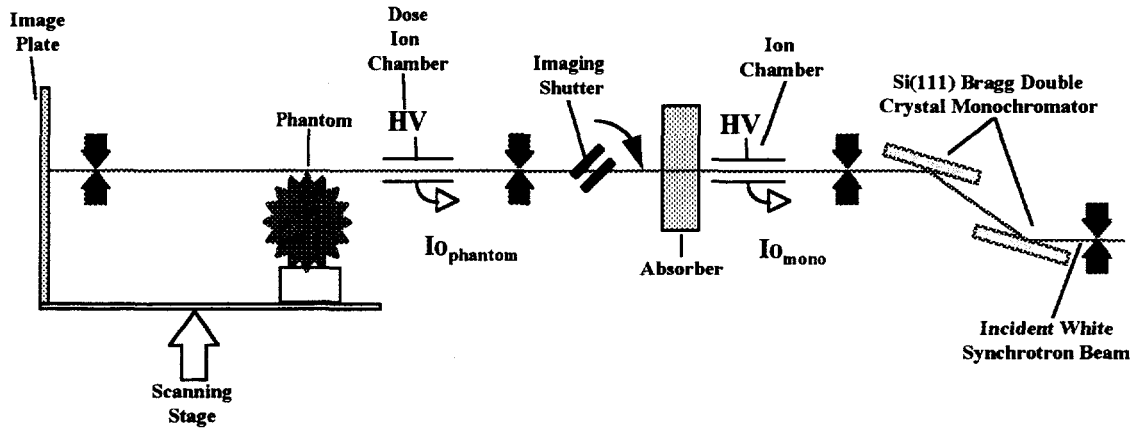

Figure 1: Mammogaphy imaging set-up (not to scale)

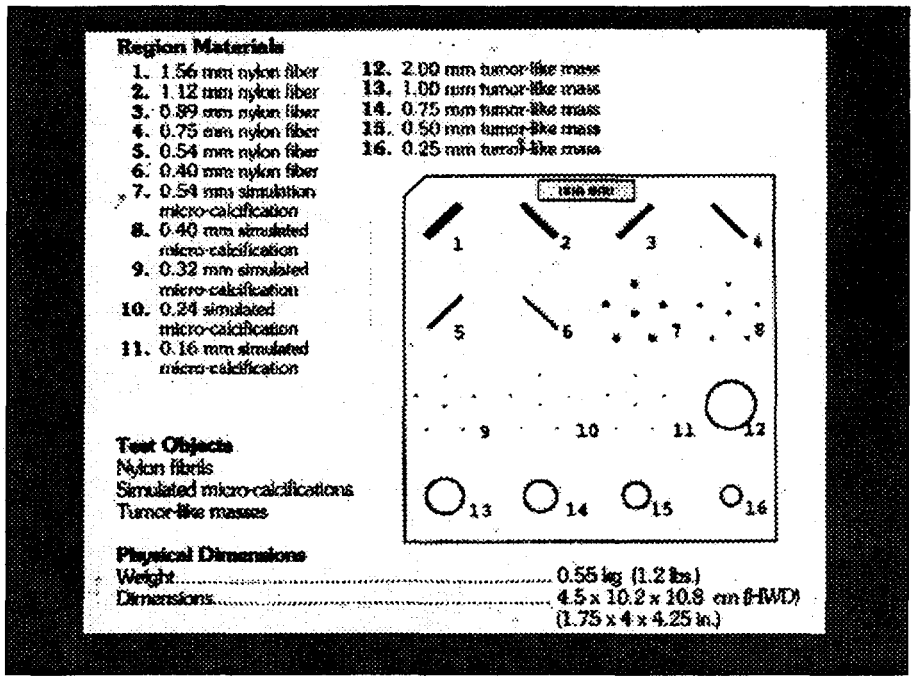

AMERICAN COLLEGE OF RADIOLOGY PHANTOM

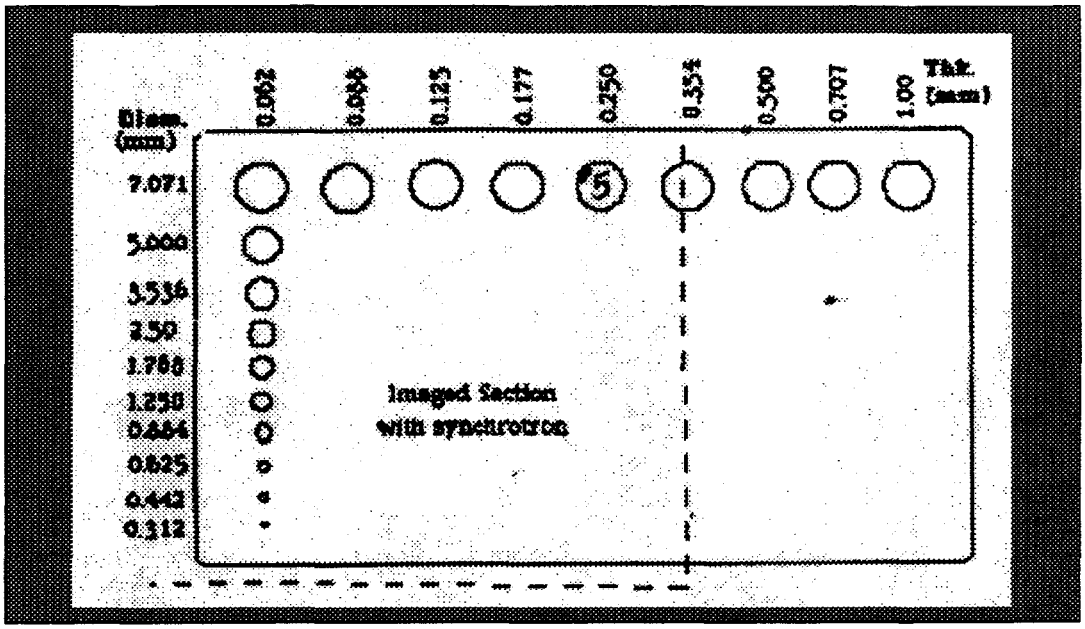

CONTRAST DENSITY PHANTOM

Figure 2: Details of the American College of Radiology Phantom and the Contrast Detail Phantom.

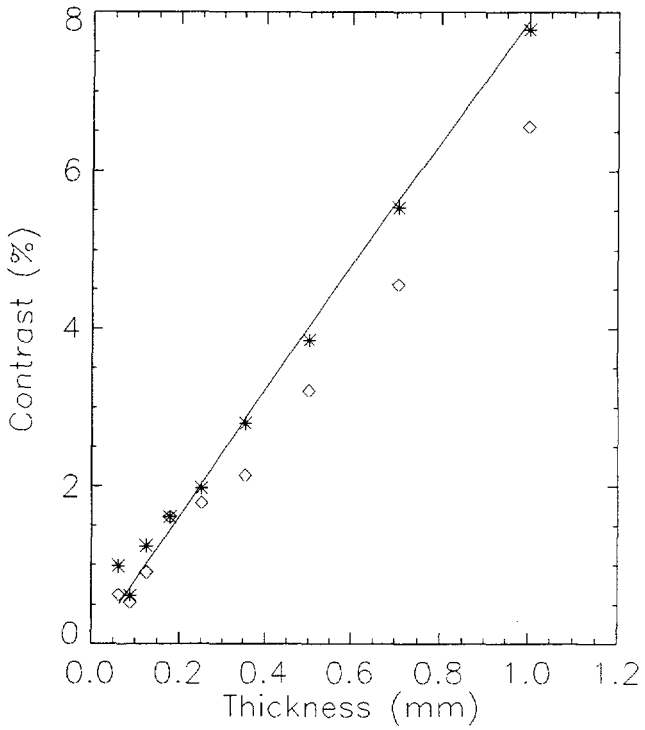

Figure 3: Measured contrast at 18 keV (*). The solid line represents the theoretical contrast. The measured contrast for a conventional film (25kVp) is also plotted (◊).

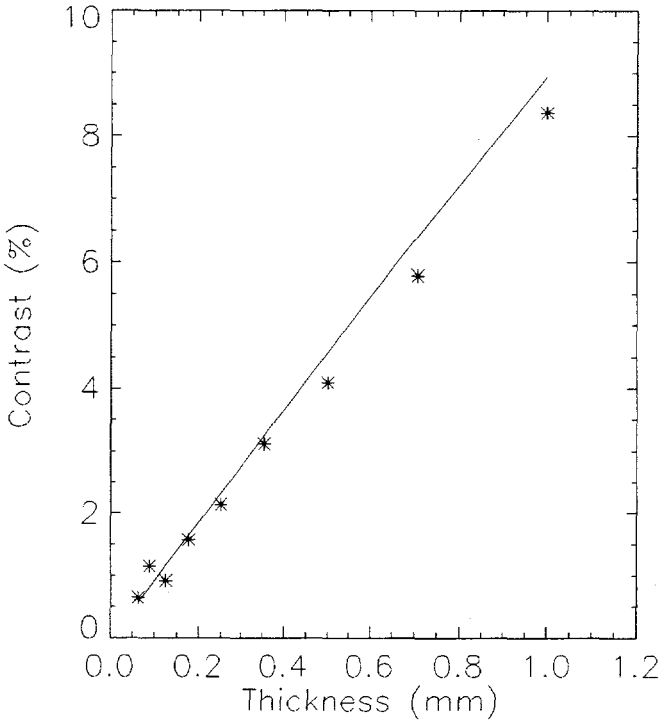

Figure 4a: Measured contrast at 17 keV (*). The solid line represents the theoretical contrast.

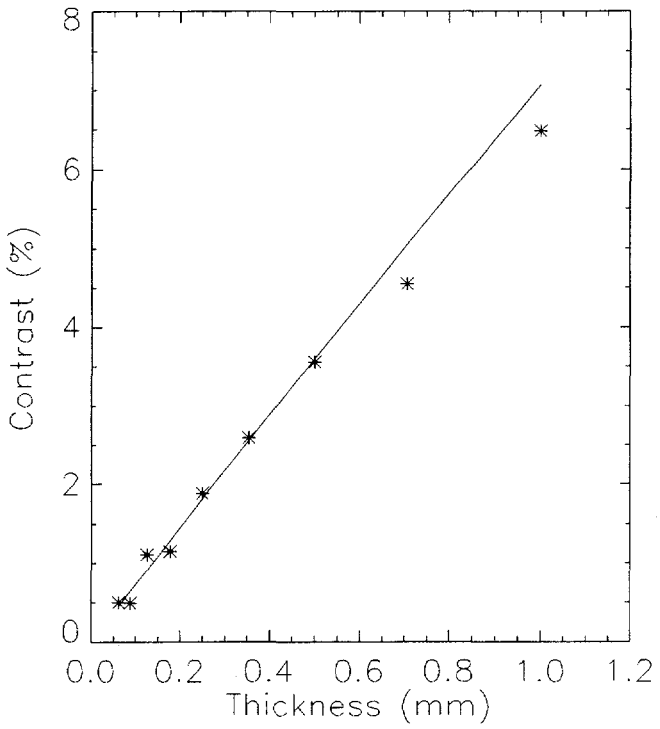

Figure 4b: Measured contrast at 19.3 keV (*). The solid line represents the theoretical contrast.

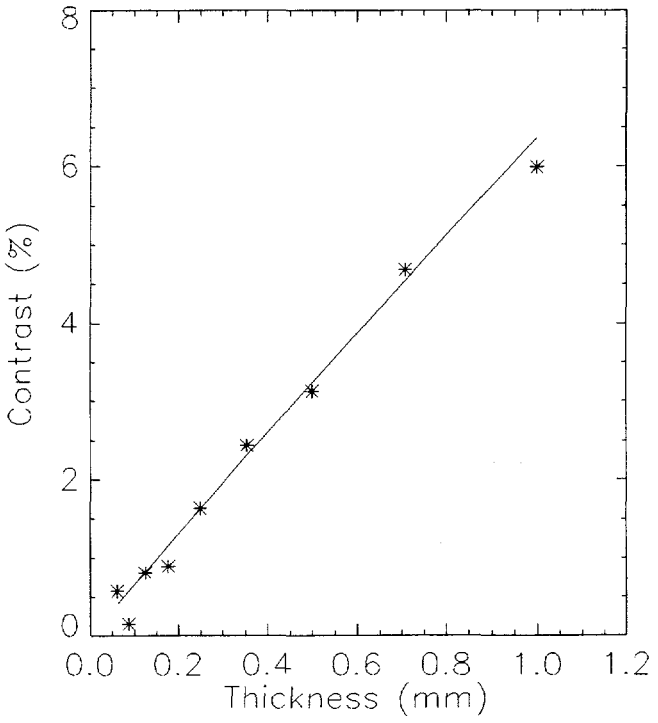

Figure 4c: Measured contrast at 20 keV (*). The solid line represents the theoretical contrast.

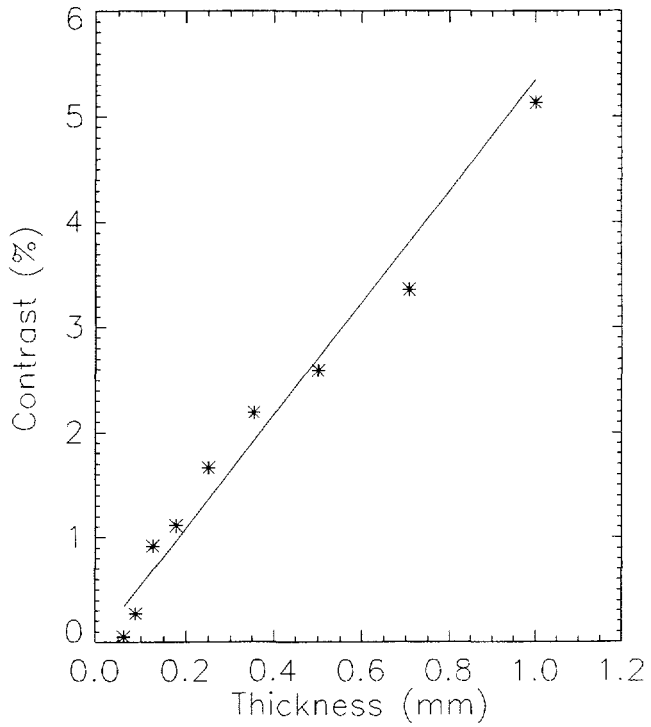

Figure 4d: Measured contrast at 22 keV (*). The solid line represents the theoretical contrast.

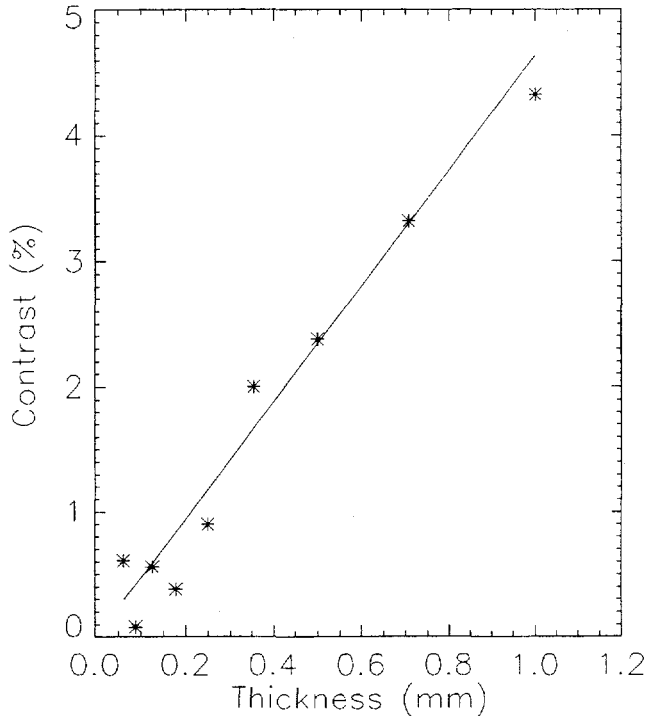

Figure 4e: Measured contrast at 24 keV (*). The solid line represents the theoretical contrast.

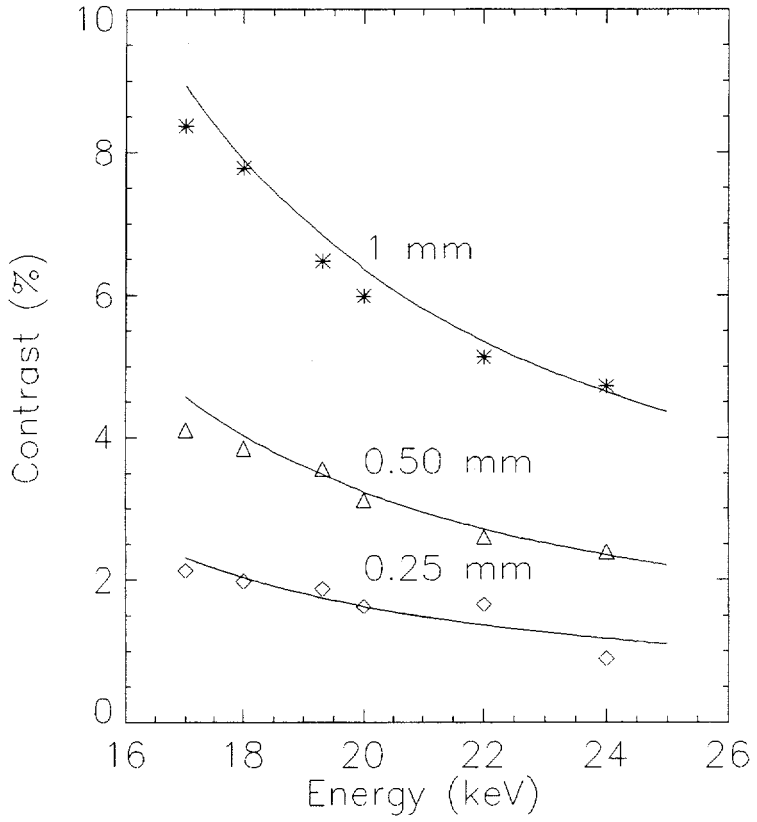

Figure 5: Measured contrast for different detail thicknesses. The solid line represents the theoretical contrast.